fibers

MDPI

Article

Multifunctional, Flexible, Electrospun Lignin/PLA Micro/Nanofiber Mats from Softwood Kraft, Hardwood Alcell, and Switchgrass CELF Lignin

Dorota B. Szlek *, Emily L. Fan and Margaret W. Frey

Department of Human Centered Design, Cornell University, 37 Forest Home Drive, Ithaca, NY 14853, USA; elf77@cornell.edu (E.L.F.); mfw24@cornell.edu (M.W.F.)
* Correspondence: ds969@cornell.edu

Highlights

What are the main findings?

- Lignin origin, isolation method, and fraction significantly influence fiber properties of electrospun 1:1 lignin/PLA micro/nanofibers, including spinnability, morphology, mechanical strength, thermal behavior, hydrophobicity, and antioxidant activity.
- Fractionation is not essential for fiber formation, but it enables tailoring of fiber properties to achieve targeted performance characteristics

What is the implication of the main finding?

- Lignin/PLA fiber mats can be customized for diverse functionality: in this study, SGL/PLA demonstrated suitability for air filtration systems, KL/PLA for wound dressings or cosmetic care, and Alcell/PLA for packaging applications.
- Efficient, low-cost production of functional biocomposite micro/nanofibers is feasible, supporting sustainable material development without complex processing, while enabling targeted performance through selective lignin use or fractionation

Abstract

Herein, biobased 1:1 lignin/polylactic acid (PLA) blends are electrospun into micro- and nanofiber mats. Lignin samples originating from softwood, hardwood, and switchgrass biomass, extracted through the Kraft, Alcell, and CELF processes, respectively, and processed into soluble and insoluble fractions, are used. Functional properties of the mats varied with lignin biomass origin, isolation method, and fraction. Mat attributes are demonstrated through analysis of spinnability, thermal and mechanical behavior, chemical structure, morphology, hydrophobicity, and antioxidant activity. Samples spun with hardwood Alcell lignin fractions were brittle and rigid with the highest Young's modulus, lowest elongation at break, and hydrophobic contact angle > 100°. Switchgrass CELF lignin (SGL)/PLA mats showed the highest tensile strength, a low Young's modulus, and high elongation at break, as well as good spinnability with the smallest fiber diameter from all samples. Kraft lignin/PLA demonstrated similar mechanical properties to SGL/PLA, as well as the highest antioxidant activity, measurable within 5 min. Therefore, while they did not dictate spinnability, the lignin biomass origin and pretreatment method were shown to have a significant impact on fiber properties, while the use of lignin fractions was shown to tailor functional properties of fibers for specific end use, such as in flexible, hydrophobic, or antioxidant product applications.

check for updates

Academic Editors: Ramiro Rafael Ruiz Rosas and Francisco José García-Mateos

Received: 6 August 2025
Revised: 6 September 2025
Accepted: 15 September 2025
Published: 19 September 2025

Citation: Szlek, D.B.; Fan, E.L.; Frey, M.W. Multifunctional, Flexible, Electrospun Lignin/PLA Micro/Nanofiber Mats from Softwood Kraft, Hardwood Alcell, and Switchgrass CELF Lignin. *Fibers* **2025**, *13*, 129. https://doi.org/10.3390/fib13090129

Copyright: © 2025 by the authors. Licensee MDPI, Basel, Switzerland. This article is an open access article distributed under the terms and conditions of the Creative Commons Attribution (CC BY) license (https://creativecommons.org/licenses/by/4.0/).

Keywords: lignin; Kraft; organosolv; CELF; Alcell; nanofibers; electrospinning

1. Introduction

Advances in processing technologies have contributed to biomass becoming a viable feedstock alternative to petroleum in the synthesis of chemical products, including man-made fibers. Lignin is known for hydrophobicity, thermal stability, rigidity, and UV absorbance, as well as antioxidant and antibacterial properties. It is the second most abundant renewable biopolymer on earth and can be isolated from native woody (including softwood and hardwood species) and herbaceous plants, as well as agricultural, paper-making, and biorefinery waste [1]. The benefits of using lignin biomass in fiber manufacturing lie in its biodegradability, renewability, and a multitude of inherent functional properties. However, its branched and heterogenous structure and solubility will differ based on the lignin source, making it difficult to process [2,3].

Lignin can be extracted via biological/enzymatic, physical, or chemical methods. The Kraft and organosolv processes are both examples of chemical methods, and the latter includes sub-categories, such as Co-Solvent Enhanced Lignocellulosic Fractionation (CELF) and the ethanol-based Alcell process [1]. The type of chemicals used and temperature, pressure, and duration of processing all affect lignin properties [4]. Phenolic hydroxyl group and aliphatic hydroxyl group contents of lignin are strongly influenced by the isolation conditions. The hydroxyl groups influence thermal and physical properties of lignin via intra- and intermolecular hydrogen bonding. Hydrogen bonds can also cause steric hindrance, reducing the accessibility of other functional groups in lignin [5]. The specific extraction processes investigated in this study are Kraft, Alcell, and CELF. Kraft lignin is a byproduct of the Kraft pulping process based on acid hydrolysis and resulting in formation of C-C linkages and a degraded and highly condensed lignin structure [1,6]. CELF pretreatment uses acidic aqueous tetrahydrofuran (THF) mixtures, and while the extracted lignin quality and structure heavily depend on processing conditions, temperature, duration, and acid content, resulting lignin has a high free phenolic OH group content [6,7]. In the Alcell process, lignin is isolated with ethanol as the organic solvent and is characterized by a high purity, as well as a higher phenolic/aliphatic OH content, compared to alkali lignins [8,9].

Biomass species and origin also impact lignin chemical structure. Lignin is amorphous with a branched structure of alkylphenolic rings, resulting from a combination of three aromatic structural units. The ratio of syringyl (S), guaiacyl (G), and p-hydroxyphenyl (H) units (Figure 1) is dictated by lignin biomass origin [10–12]. Softwood lignin is mainly composed of G units, hardwood lignin is composed of S and G units, and herbaceous lignin is characterized by a large quantity of H units in addition to S and G units [12].

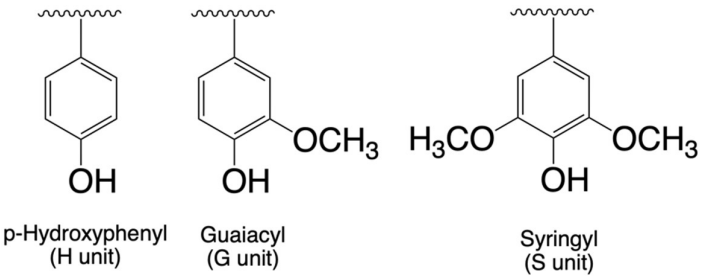


Figure 1. The chemical structures of S, G, and H monolignols.

Electrospinning is an electrohydrodynamic process during which fibers are produced from a polymer solution through elongation, chain entanglement, and solvent evapo-

ration under applied voltage [13,14]. Electrospinning lignin is very difficult because of its branched structure, heterogeneity, and low molecular weight. Hence the addition of other polymeric systems is common to facilitate lignin-based micro/nanofiber spinning [13]. Most studies on electrospinning of 100% lignin have not resulted in any fiber formation [15]. Formation of bead-on-string structures or electro spray has been attributed to the highly branched lignin structure and lack of molecular chain entanglement in the spinning solution [15]. To improve the spinning process, an easily spinnable polymer, such as polyethylene oxide (PEO), polyvinyl alcohol (PVA), polylactic acid (PLA), polycaprolactone (PCL), and others, has been added to facilitate the electrospinning of lignin-based fibers [16–18]. In particular, polylactic acid (PLA) is a commercially compostable aliphatic polyester that has good mechanical properties but poor thermal stability [19]. A blend of PLA and lignin can potentially enhance spinnability and tensile properties of lignin and thermal stability of PLA, while also increasing hydrophobic, antibacterial, antioxidant, and UV resistance properties, which have been demonstrated in several studies [20–22]. However, most studies on lignin/PLA composite fiber mats focus on specific applications using a single type of lignin [21,23,24] rather than on systematic comparisons of fiber properties across lignins of different biomass origins, pretreatment methods, or fractions. While a few studies conducted such comparisons, they often employed alternative spinning methods or blended lignin with copolymers other than PLA [25,26]. Research specifically examining electrospun lignin/PLA fibers in relation to the lignin origin, isolation method, or fraction remains limited, and the diversity of lignin types explored in these studies is notably narrow [16,27]. Additionally, to authors' knowledge, this is the first study that includes photographs of the tangible micro/nanofiber lignin/PLA mats.

In this study, lignin was mixed with PLA in 50:50 ratio in a mixed efficient solvent system of N, N-Dimethylformamide (DMF) and Dichloromethane (DCM) in a 2:7 ratio. Lignin originating from three different categories of biomass, hardwood, softwood, and grass, and extracted by three methods, Kraft, CELF, and Alcell, was used. To understand the impacts of solubility and substructure on spinnability and properties, lignin was fractionated into soluble and insoluble fractions. Lignin samples were suspended in PLA/DMF/DCM solutions and electrospun into micro- and nanofiber mats. Variability of suspension spinnability and resulting fiber properties between the lignin-based samples were documented. Appropriate correlations between these factors and suspension and spinning parameters, such as conductivity, thermal and mechanical behavior, chemical structure, and morphology, were further measured and analyzed. Recommendations of select lignin types for specific applications were provided.

2. Materials and Methods

2.1. Materials

Kraft lignin (softwood, pine) was purchased from Sigma-Aldrich (St. Louis, MO, USA). ACS-grade acetone and HPLC-grade MeOH were purchased from Fisher Chemical (Waltham, MA, USA). Two-hundred-proof pure ethanol was purchased from Koptec (King of Prussia, PA, USA). Anhydrous 99.8% N, N-Dimethylformamide (DMF) was purchased from Sigma-Aldrich (St. Louis, MO, USA). Extra dry, stabilized 99.9% Dichloromethane (DCM) was purchased from Acros Organics (Fair Lawn, NJ, USA). Fiber-grade 6252D polylactic acid (PLA) pellets were purchased from NatureWorks® Ingeo™ (Blair, NE, USA). DPPH was purchased from Cayman Chemical Company (Ann Arbor, MI, USA).

2.2. Fractionation

Kraft lignin was fractionated into soluble and insoluble fractions with ethanol or acetone using gravimetric filtration and rotary evaporator, as per an earlier work [28].

Alcell lignin, supplied by the State University of New York College of Environmental Science and Forestry (Syracuse, NY, USA), was isolated from hardwood chips using the organosolv process and fractionated with ethanol into 40% ethanol, 60% ethanol, and 100% ethanol-soluble fractions, as well as an 100% ethanol-insoluble fraction. Switchgrass lignin, supplied by the Chmely Biomaterials Chemistry Laboratory from the Pennsylvania State University (University Park, PA, USA), was isolated using Co-Solvent Enhanced Lignocellulosic Fractionation (CELF) from 1 mm dried and milled switchgrass particles. Both, soluble and insoluble lignin fractions were used to prepare spinning dopes.

2.3. Suspension Preparation

Suspensions containing PLA:lignin 50:50 by weight were prepared by first separately suspending 1 g of lignin in 2 mL of DMF and dissolving 1 g of PLA in 7 mL of DCM and shaking for 1 h on a Burrell wrist-action shaker. The lignin and PLA suspensions/solutions were combined and shaken overnight to form a resulting 22% w/v suspension. The lignin/PLA ratios were optimized in this study, identifying the 50:50 blend as having the highest lignin content while retaining the most favorable spinnability.

2.4. Electrospinning

Spinning parameters were optimized at a 3 mL/h flow rate, 20 cm distance to the collector, and 20 kV applied voltage. The horizontal electrospinning setup included the Gamma High Voltage Research, Inc. HV power supply (Ormond Beach, FL, USA) and Harvard Apparatus, Inc. PHD/ULTRA syringe pump (Holliston, MA, USA). Beckton, Dickinson and Company (BD) syringes (5 mL) (Canaan, CT, USA) were used in combination with a BD PrecisionGlide 21G needle (Franklin Lakes, NJ, USA). The collector was a copper plate covered with aluminum foil and placed across from the syringe in a Plexiglas box. Relative humidity and temperature were not controlled but recorded and ranged from 64.2 to 69.9% and 19.6–21.2 °C. Micro/nanofiber mats were collected from different lignin blends with PLA 5 min after initiation of the pump and the voltage system.

2.5. Scanning Electron Microscopy (SEM) Analysis

Scanning Electron Microscopy (SEM) was utilized to study the morphology and surface topology of lignin/PLA fiber mats. Micrographs of electrospun fiber mats were obtained with Carl Zeiss AG LEO 1550 Field Emission Scanning Electron Microscope (FE-SEM) (Oberkochen, Germany), using Carl Zeiss AG InLens and SE2 detectors (Oberkochen, Germany), at an acceleration voltage of 3 kV and working distance of 6 mm. Prior to SEM analysis, each sample was coated with Au/Pd for 90 s using a Quorum Technologies Ltd. SC7620 sputter coater (East Grinstead, UK) under a vacuum.

2.6. Fiber Diameter Measurement

The fiber diameter was analyzed using micrographs from SEM Keck (FEI Company, Hillsboro, OR, USA). Next, ImageJ.JS software (version 1.54p) was used to measure the diameter of one hundred fibers in each sample, using a reference scale bar. The average fiber diameter was calculated for each sample based on this data, along with the standard deviation.

2.7. Attenuated Total Reflectance (ATR)—Fourier-Transform Infrared Spectroscopy (FTIR)

FTIR spectra were collected using a FTIR-ATR Perkin Elmer Spectrum spectrometer (Perkin Elmer, Waltham, MA, USA). Triplicate measurements were collected in the wavelength range from 4000 to 600 cm^{-1} with a resolution of 4 cm^{-1} and a total of 16 scans.

2.8. Differential Scanning Calorimetry (DSC)

Thermal analysis was performed using a Differential Scanning Calorimetry (DSC) Q2000, V24.9, Build 121 instrument from TA Instruments (New Castle, DE, USA). Nanofiber samples were sealed in an aluminum T-zero pan (TA Instruments, New Castle, DE, USA) with a hermetic lid, cooled to a temperature of 20.00 °C (from 40 °C), kept isothermal for 1.00 min, and then heated to 200.00 °C at a rate of 20.00 °C/min under a nitrogen atmosphere with a flow rate of 50 mL/min. The sample weight range was 0.677–1.498 mg.

2.9. Characterization of Mechanical Properties

TA Instruments Dynamic Mechanical Analysis (DMA) Model Q800DMA (New Castle, DE, USA) was used to obtain the stress/strain curve of those lignin/PLA samples that were able to form micro/nanofiber mats, with neat PLA as the control sample. From that data, tensile strength, modulus, elongation, and breaking strength were obtained. Testing was performed in triplicate using samples at a ramp force of 0.1 N/min, as shown in Figure 2. The thickness of each tested strip was measured using Mitutoyo Digimatic Indicator Type IDF-112E (Aurora, IL, USA), with a measurement range of 12 mm, resolution of 0.001 mm, and an accuracy of ±0.003 mm at three points, and then averaged, ranging from 0.026 to 0.134 mm.



(**a**) (**b**)

Figure 2. Image of KL/PLA NF sample positioned in clamp (**a**) before tensile testing and (**b**) after testing was completed.

2.10. Contact Angle Analysis

Water contact angle measurement was carried out using the Droplet Lab smartphone-based tensiometer (Toronto, ON, Canada) with the Sessile drop method under ambient conditions. A droplet of deionized water was generated on the surface of each sample using a Hamilton Gastight #1750 syringe (Reno, NV, USA) fitted with an 18-gauge needle, and the resulting contact angle calculated using Young–Laplace fitting. Triplicate measurements were taken within 10 s by applying the water droplet in three different areas of each sample, after which the average contact angle was calculated for each sample. Contact angle analysis was performed by the Droplet Lab software (Toronto, ON, Canada) automatically at the time of measurement collection.

2.11. Antioxidant Activity

The antioxidant activity was evaluated by measuring the reduction rate of the DPPH radical in the antioxidant's presence via UV-Vis spectroscopy, using the BioTek Synergy Neo2 multimode microplate reader (Winooski, VT, USA). Additionally, the antioxidant activity of ascorbic acid was measured as the positive control and that of neat PLA as the negative control. DPPH solution in methanol (MeOH) was prepared immediately before

beginning the assay, and 2 mL of 60 µM DPPH solution in MeOH was added to each 2 mg sample vial. Samples were incubated at room temperature under light protection. Absorbance measurements at 517 nm were taken 2 h, 4 h, and 24 h after the addition of the DPPH solution to the nanofibers, conducted in 96-well microtiter plates with lids, with 100 µL of the respective sample solution mixed and then pipetted into 4 wells per time slot. The antioxidant activity of the samples was calculated using equation, based on the residual DPPH content (%) = (A0 − A1)/A0 × 100.

2.12. Statistical Analysis

Statistical significance of all results was analyzed by applying ANOVA and paired two-sided *t*-tests at a 95% confidence level between two arrays of mean values for the same sample set. In many cases, indication of low significance stemmed from the small size of the population tested.

3. Results

Although all fibers formed were 1:1 *w*/*w* PLA:lignin, significant differences in fiber morphology and properties were found as a result of lignin sample. Ten different samples were spun and coded according to lignin type and any fractionation shown in Table 1.

Table 1. Lignin with their fiber identifier, biomass origin, extraction method, and S/G ratio.

	KL	AIKL	ASKL	EIKL	ESKL	ALE40	ALE60	ALE100	ALE100INS	SGL
Biomass Source	softwood	softwood	softwood	softwood	softwood	hardwood	hardwood	hardwood	hardwood	switchgrass
Isolation Method	Kraft lignin as received	Acetone-Insoluble Kraft Lignin	Acetone-Soluble Kraft Lignin	Ethanol-Insoluble Kraft Lignin	Ethanol-Soluble Kraft Lignin	Alcell, soluble in 40% EtOH	Alcell, soluble in 60% EtOH	Alcell, soluble in 100% EtOH	Alcell, soluble in 100% EtOH	Co-Solvent Enhanced Lignocellulosic Fractionation
S/G Ratio	0.33	0.42	0.23	0.53	0.29	1.46	1.30	1.49	1.59	0.25
Fiber Label	KL/PLA	AIKL/PLA	ASKL/PLA	EIKL/PLA	ESKL/PLA	ALE40/PLA	ALE60/PLA	ALE100/PLA	ALE100INS	SGL/PLA

3.1. Chemical Structure (FTIR)

FTIR was used to identify the presence of S, G, and H monolignols in each sample, to compare the S/G ratio, degree of crosslinking, and total OH group content among samples, and to check for the presence of any impurities.

The aromatic skeleton vibrations visible at 1600, 1515, and 1426 cm^{-1}, as well as the intense bands at 2948 and 2863 cm^{-1} representative of CH and methoxy groups, are characteristic of all lignins, but presented with varying intensities. The vibration at 1705 cm^{-1} in the carbonyl/carboxyl region was observed not only for all Alcell lignin samples, due to its association with solvent-extracted hardwood lignins [29], but also for the ESKL lignin, most likely pointing to the solvent-soluble softwood KL fractions being sulfur-free. Additionally, vibrations in the 1000–1300 cm^{-1} region are visible in all samples and may signify the presence of carbohydrate impurities [29]. However, they are especially pronounced in all Alcell lignins and in the ESKL fraction.

Relative S/G ratios were calculated for all samples using methods developed by Popescu et al. (2006), Del Rio et al. (2007), and Sammons et al. (2013), focused on the 1325 cm^{-1} peak representing S units and the 1270 cm^{-1} peak representing G units (Figure 3b–d) [30–32]. Due to the prevalence of G units in softwood Kraft lignin, S/G ratios were quite low in contrast with hardwood Alcell lignin, which contained both G and S units, with a significantly larger S unit content. Switchgrass CELF lignin contained a larger amount of G units, similar to softwood Kraft lignin, but also contained H units characteristic of herbaceous lignins (Figure 3c,d; Table 1) [33,34]. Additional peaks at

814–817, 855, 1140, and 1154–1152 cm^{-1}, representative of G units, at 1127–1124 and 1597–1593 cm^{-1}, representative of S units, and at 882 cm^{-1}, indicating the presence of H units, further support this interpretation (Figure 3b–d) [32,35,36]. The differences in relative S/G ratios between the samples with different lignins had direct implications on the thermal behavior, as well as mechanical properties and antioxidant activity, of the fiber mats, as discussed in Sections 3.3, 3.4 and 3.6.

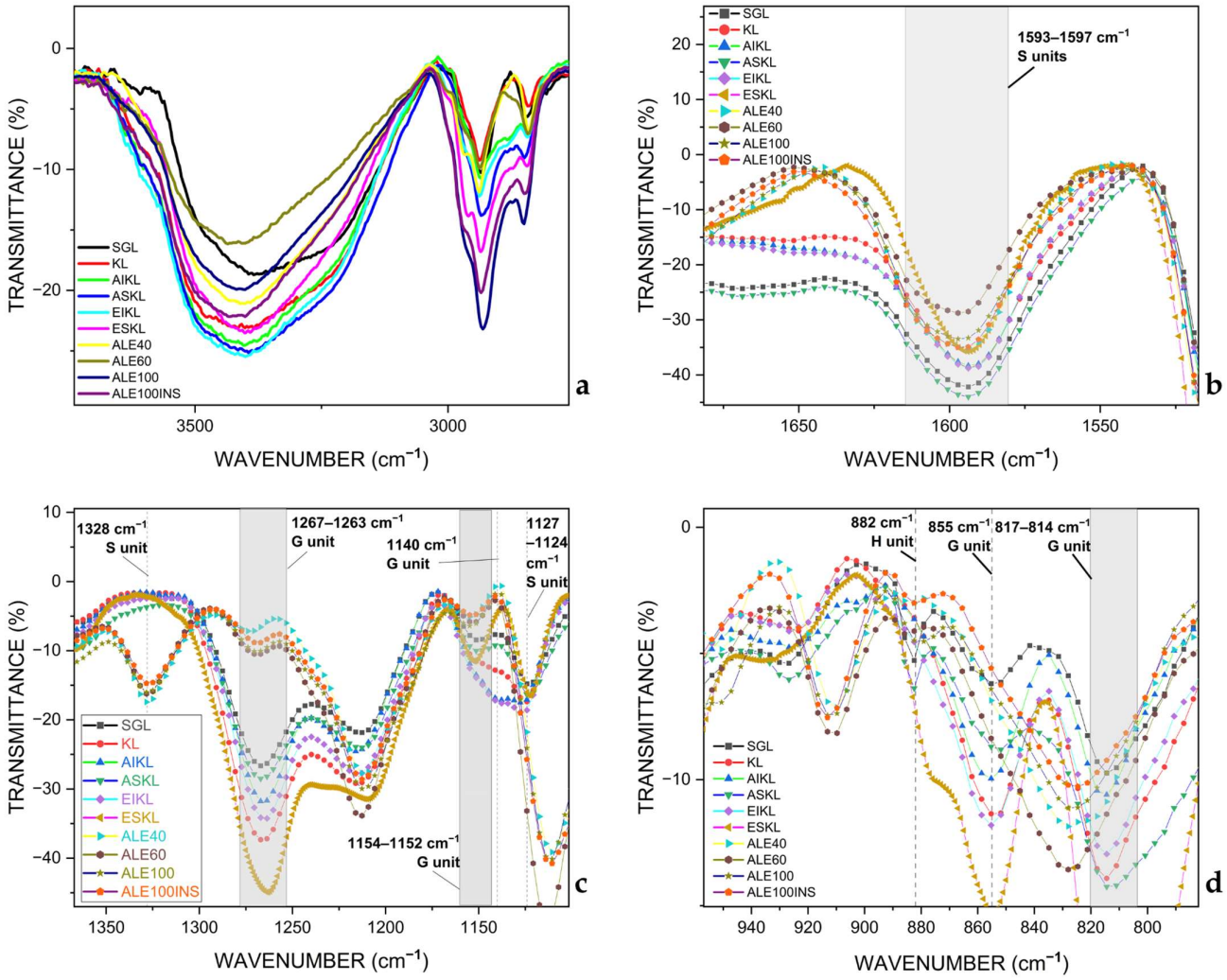


Figure 3. Closeup views of the FTIR spectra representing (**a**) hydrogen bonding/total OH content; and (**b**–**d**) S, G, and H units in lignin along with the lignin's S/G ratios.

The band at ~3400 cm^{-1} is linked to aromatic and aliphatic OH groups in lignin (Figure 3a) [32,37]. The amount of OH groups can define lignin reactivity and, effectively, its potential for use in targeted applications [38]. Integration of the bands in the hydroxyl stretching region across all lignin samples produced relative peak areas representing intermolecular hydrogen bonding and the associative total OH content in lignin [39–41]. Simultaneously, the relative ratio of absorbance intensities of the ~1500 and ~1600 cm^{-1} peaks, representing aromatic ring breathing, was calculated for all lignin samples, following the method outlined by Mann et al. (2009), to estimate the degree of crosslinking/condensation in lignin [42]. The degree of crosslinking here refers to interunit carbon–carbon bonds at free C5 and C6 positions of a phenolic hydroxyl unit [43]. These values corresponded inversely to the relative hydrogen bonding/total OH content in lignin (Figure 4). This inverse relationship has also been previously demonstrated by de Souza Junior et al. (2018) [36] and is further supported by thermal analysis and contact angle measurements. A strong negative

correlation coefficient was observed between the relative ~3400 cm^{-1} peak area—associated with hydroxyl groups and hydrogen bonding—and both the glass transition temperature T_g ($r = -0.70$) and melting temperature T_m ($r = -0.77$) of lignin/PLA composite fibers. This suggests that increased OH bonding/OH content are inversely related to thermal properties of the fibers, which has been demonstrated in earlier studies [44]. Additionally, although moderate due to other contributing factors, a negative correlation was also found between the relative ~3400 cm^{-1} peak area and contact angle measurements ($r = -0.43$), indicating that higher OH content slightly reduces hydrophobicity. Overall, these inverse relationships between OH bonding/content and the degree of crosslinking, thermal properties, and contact angle suggest that lower OH content reduces lignin reactivity in these samples, promoting the formation of more rigid, hydrophobic, and thermally stable fiber mats.

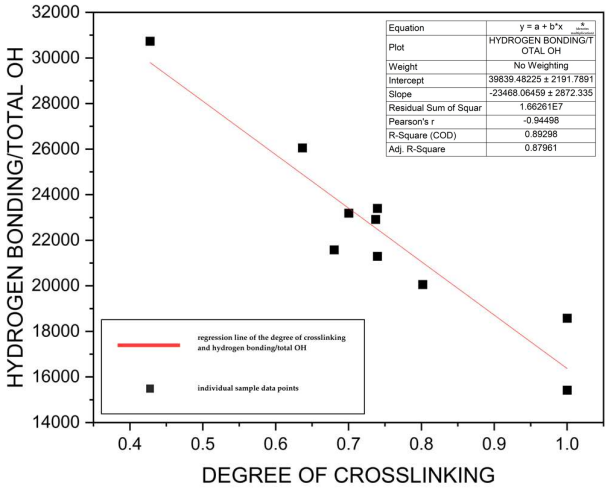


Figure 4. Regression line of the degree of crosslinking and hydrogen bonding/total OH content in lignin samples showing an inverse relationship.

3.2. Fiber Diameter, Distribution and Morphology

Normally, the increase in conductivity (Table 2 yields a decrease in fiber diameter, but the addition of lignin with its highly branched molecular network to PLA resulted in an increase in the fiber diameter instead. Although all samples successfully produced continuous micro- and nanofibers (Figure 5), the addition of lignin to PLA increased the average fiber diameter in all samples, as expected from the addition of a highly branched molecule (Table 3, Figure S1). A possible explanation for this is the increased solution viscosity from the number of solute–solute interactions that arise from the entanglements of the branched groups [45]. Additionally, Kraft lignin samples had the highest diameter distribution of all samples, while ALE60/PLA and SGL/PLA had the lowest. SGL/PLA fibers were observed to spin with relatively even coverage into fibers with the lowest fiber diameter on average (Table 3, Figure S1), which has been noted with other switchgrass-derived spun fibers [46]. This pattern correlates with the solubility of lignin in the DMF/DCM solvent system, governed by the pretreatment method and fraction. In support of this argument, ASKL/PLA fibers also showed a low average fiber diameter (Table 3) due to the use of the soluble fraction, comparable to that of SGL/PLA, where superior solubility of organosolv lignin in organic solvents dictated the smaller fiber diameters [47]. While the fiber diameter distribution data for the other samples was not found to be statistically significant, solubility, driven by lignin dispersion in the PLA matrix and hydrogen bonding/OH content, had a strong influence on the diameter of produced fibers.

Table 2. Conductivity of lignin/PLA and PLA control suspensions.

	KL/PLA	AIKL/PLA	ASKL/PLA	EIKL/PLA	ESKL/PLA	ALE40/PLA	ALE60/PLA	ALE100/PLA	ALE 100INS/PLA	SGL/PLA	PLA
Conductivity (μS/cm)	20.40 ± 1.69	18.38 ± 2.07	23.03 ± 2.76	14.90 ± 1.47	27.07 ± 2.10	21.35 ± 2.62	12.41 ± 1.15	9.31 ± 0.75	7.17 ± 1.28	16.33 ± 0.82	1.57 ± 0.37

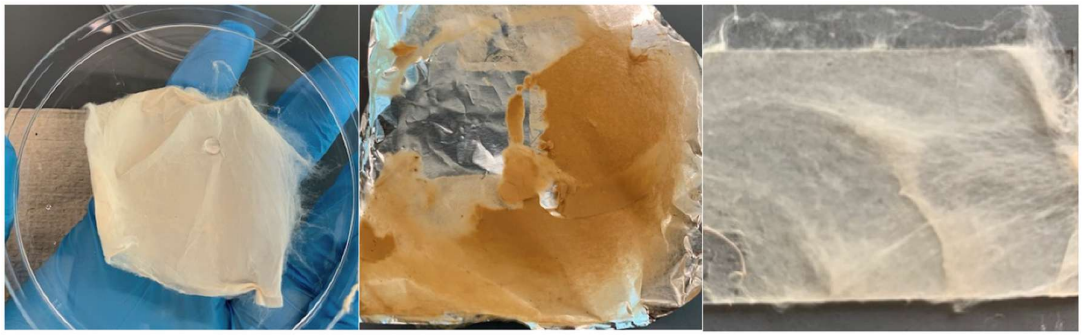


Figure 5. Micro/nanofiber mats. From left: KL/PLA, ALE60/PLA, and SGL/PLA. Color of the lignin mats was influenced by chromophore content, determined by lignin biomass origin, isolation method, and fraction.

Table 3. Lignin/PLA and neat PLA fiber mats with their tested properties. * Blanks indicate samples not tangible/strong enough to be mounted in the DMA clamps.

Fiber Label	T_g (°C)	T_{cc} (°C)	T_m (°C)	Enthalpy of Fusion (J/g)	Ultimate Tensile Strength (MPa)	Young's Modulus (MPa)	Elongation at Break (%)	Average Water Contact Angle (°)	Antioxidant Activity (%)	Average Fiber Diameter (μm)
KL /PLA	57 ± 0.3	79 ± 0.3	151 ± 0.3	26.07 ± 16.32	0.37 ± 0.05	0.19 ± 0.04	7.75 ± 6.22	131.37 ± 4.56	55.21 ± 1.96	1.38 ± 0.34
AIKL /PLA	56 ± 1.7	73 ± 0.5	153 ± 0.3	35.01 ± 14.63	0.23 ± 0.09	0.07 ± 0.03	39.66 ± 21.83	114.47 ± 1.86	55.25 ± 1.59	1.32 ± 0.44
ASKL /PLA	56 ± 1.2	73 ± 0.3	154 ± 1.1	32.96 ± 9.17	0.15 ± 0.02	0.03 ± 0.00	17.34 ± 4.08	126.72 ± 1.14	56.46 ± 1.61	0.87 ± 0.63
EIKL /PLA	57 ± 0.8	75 ± 1.6	154 ± 1.8	37.48 ± 2.53	0.38 ± 0.11	0.11 ± 0.01	18.49 ± 5.55	125.66 ± 7.06	56.54 ± 1.17	1.12 ± 0.43
ESKL /PLA	43 ± 1.62	68 ± 0.42	143 ± 3.66	25.84 ± 9.18	*	*	*	110.62 ± 2.30	47.15 ± 1.56	1.33 ± 0.36
ALE40 /PLA	56 ± 4.4	77 ± 5.9	150 ± 3.0	18.48 ± 3.56	*	*	*	122.09 ± 6.52	33.66 ± 1.16	1.37 ± 0.45
ALE60 /PLA	56 ± 0.6	74 ± 0.7	152 ± 2.3	18.45 ± 6.14	0.35 ± 0.17	0.25 ± 0.08	1.33 ± 0.22	138.67 ± 4.37	32.90 ± 1.15	1.44 ± 0.23
ALE100 /PLA	55 ± 0.9	73 ± 1.3	151 ± 1.3	21.63 ± 5.18	*	*	*	115.76 ± 2.75	27.41 ± 1.64	1.36 ± 0.34
ALE100 INS/PLA	57 ± 0.3	78 ± 0.8	151 ± 0.6	19.53 ± 5.33	0.18 ± 0.15	0.23 ± 0.14	13.56 ± 15.16	136.16 ± 5.10	21.12 ± 1.70	1.37 ± 0.48
SGL /PLA	56 ± 1.5	74 ± 2.1	153 ± 1.6	31.22 ± 0.74	0.44 ± 0.39	0.15 ± 0.02	26.36 ± 6.32	130.26 ± 2.63	37.05 ± 0.86	0.88 ± 0.23
PLA	58 ± 0.3	74 ± 1.0	158 ± 0.7	41.52 ± 9.42	1.70 ± 0.36	0.10 ± 0.02	74.45 ± 10.54	110.75 ± 2.98	29.46 ± 7.86	0.49 ± 0.29

In terms of morphology, in comparison to the PLA control sample, SEM micrographs of the composite fibers containing lignin all exhibited a wrinkled and porous surface morphology (Figure 6a,c) due to the rapid solvent evaporation during electrospinning and the relatively high ambient humidity. However, dense mats of continuous micro- and nano-scale fibers without beading were produced. Interestingly, SEM micrographs of Alcell lignin samples showed cracked lignin fiber cores encased in a more flexible PLA skin (Figure 6b), in line with the more rigid structure of hardwood lignin [38]. Images of SGL/PLA samples clearly showed dense networks of nanofibers, characterized by a fairly uniform diameter (Figure 6d).

3.3. Thermal Properties (DSC)

The glass transition onset temperature of all lignin/PLA blends, as well as the impact of different lignin sources on the onset of the melting point and cold crystallization behavior of PLA, were studied.

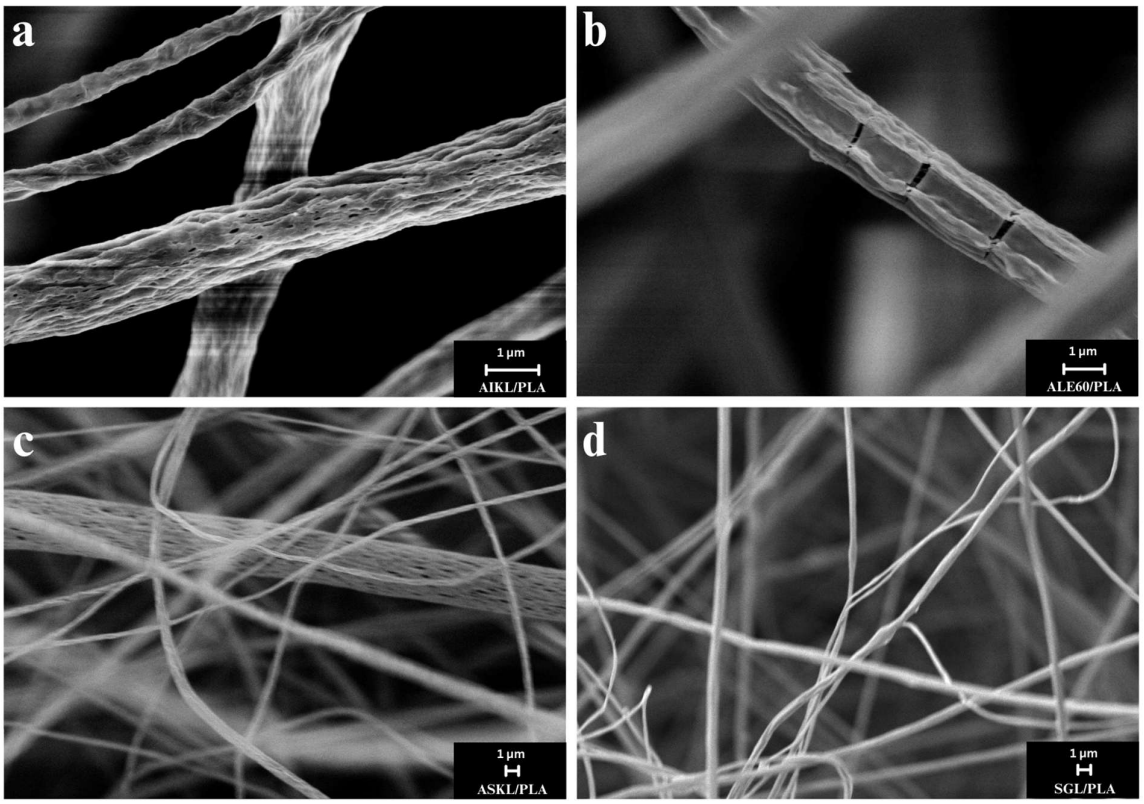


Figure 6. SEM micrographs: (**a**) AIKL/PLA, (**b**) ALE60/PLA, (**c**) ASKL/PLA, and (**d**) SGL/PLA.

While a wide range of glass transition temperatures (T_g) have been reported for lignin, ranging between 97 °C (for organosolv lignin) [48], 146 °C (for softwood organsolv lignin) [49], 108 to 154 °C (for hardwood KL) [50,51], and 160°C (for softwood KL) [26] as some examples, ultimately that value will be dictated by the lignin molar mass, biomass source, type of linkages, and their quantity, as well as heating rate [52,53]. In this study, blending PLA and lignin significantly lowered T_g to a 39.19–57.27 °C range, which is below neat PLA's T_g of 58.42 °C (Table 3, Figure 7). This pattern was consistent with findings for other lignin/PLA thermal studies [54] and can be explained by the presence of molecular interactions between the two polymers and/or a plasticization effect. It is most likely not due to phase separation, as the single T_g peak showed miscible blend behavior for all samples [50,55]. Although many polymers are immiscible with lignin due to the competing stronger interactions between lignin molecules, some polymers, like PLA, can interact with lignin through secondary forces, like hydrogen bonding, enhancing the blend's miscibility [38].

While for most samples, the change in values is subtle, data for the ESKL/PLA sample were statistically significant ($p < 0.05$) and showed not only the lowest T_g, but also the lowest T_{cc} and T_m (Table 3), which may be due to the strong hydrogen bonding interactions at the aliphatic γ- OH site between lignin and the highly polar solvent (ethanol) used during fractionation [28]. In contrast, KL/PLA and ALE100ins/PLA samples had the two highest T_g values (Table 3). Overall, the differences in thermal behavior of ethanol-fractionated and acetone-fractionated KL samples might be explained by the hydrogen bonding capacity of the two solvents, with δ_H = 19.4 for ethanol and δ_H = 7.0 for acetone, the latter being characterized by weaker hydrogen bonding interactions with the methoxy group and α-O atom [28]. Usually, hardwood lignin shows lower T_g due to its more linear structure and a higher ratio of β-O-4′ ether to C-C bonds, signifying decreased rigidity when compared with softwood lignin [51,56]. However, while the statistically significant values for the Alcell lignin samples, ALE60/PLA and ALE100/PLA ($p < 0.05$), are on the higher end of

the range, their values do not vary greatly from most of the other samples tested (Table 3). This can be explained by the combined impact of the biomass origin, extraction method, and fractionation on the monolignol distributions in other samples. Finally, it is important to note that assessment of the actual T_g can also be affected by the interactions between hydrogen bonds and the dehydration of lignin early in the cycle—first at ~50, then at ~110 °C, due to complex structure of lignin [5,57,58].

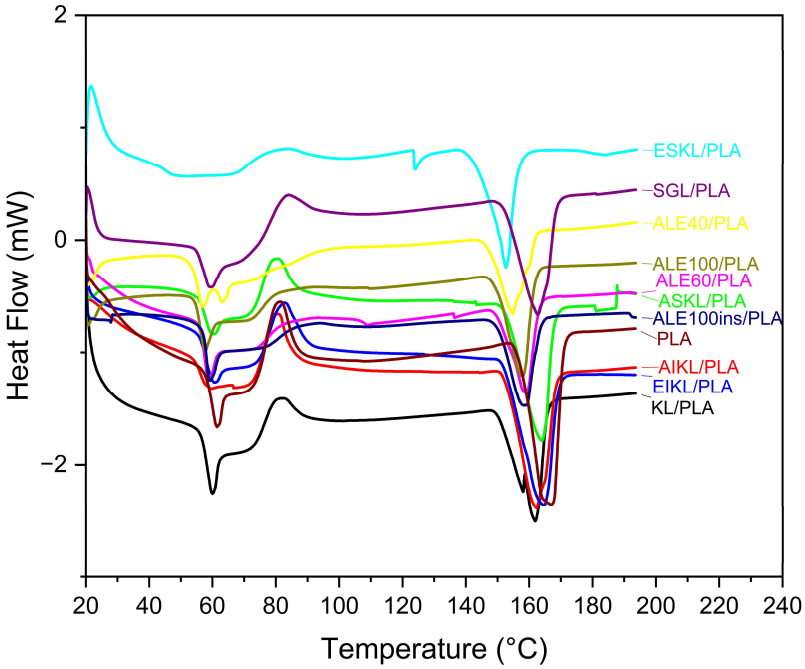


Figure 7. Thermograms of all lignin/PLA and neat PLA samples.

Additionally, as expected, a slight decrease in melting temperature (T_m), when compared with neat PLA, was observed for all samples after the addition of lignin (Table 3). Two peaks were observed for KL/PLA, with the second peak most likely resulting from melting crystallites formed during DSC characterization [19]. The lowest T_m was observed for ESKL/PLA, which was also characterized by the lowest 1597/1515 cm^{-1} peak ratios tied to crosslinking in lignin observed in FTIR spectra. Higher T_m values belonged to samples such as SGL/PLA, AIKL/PLA, ASKL/PLA, and EIKL/PLA, which also showed a higher degree of crosslinking in structural analysis.

In general, the addition of lignin to PLA resulted in a decrease in the exothermic cold crystallization peak, pointing to the incomplete crystallization of the blended polymer in fiber form [55,59]. Compared with neat PLA, the enthalpy of fusion decreased with the addition of amorphous lignin to the blends (Table 3), which was expected and signifies a decrease in nucleation density and formation of fewer crystals or incomplete crystallization [19]. Overall, the blending of hardwood organosolv (Alcell) lignin with PLA required the lowest heat of fusion when compared with Kraft softwood lignin and its fractions and CELF switchgrass lignin, which is most likely due to the highest S/G ratio values and low G unit content, pointing to increased thermal mobility [44].

3.4. Mechanical Properties (DMA)

Some of the blends (ESKL/PLA, ALE40/PLA, and ALE100/PLA) produced nanofibers, but failed to generate tangible nanofiber mats, and therefore, their mechanical properties could not be tested. However, the remainder of fibrous mats provides a cohesive representation of all lignin types sampled.

DMA tensile tests were performed to obtain stress/strain curves for all tangible nanofiber mats (Figures 7 and 8) in order to understand the impact of different lignins on the mechanical properties of lignin/PLA blends. As expected, the addition of any of the lignins to PLA resulted in the decrease in tensile strength, which has already been shown in the literature [16,60,61]. Tensile strength exhibited a high positive correlation coefficient with thermal behavior of lignins, T_g and T_m (0.78 and 0.83), and overall varied across samples, with SGL/PLA showing the highest tensile strength, followed by EIKL/PLA, KL/PLA, and ALE60/PLA, with lowest tensile strength noted in the ASKL/PLA and ALE100INS/PLA samples (Table 3). The inability of the ESKL/PLA, ALE40/PLA, and ALE100/PLA blends to form mats that can be mounted in clamps for DMA testing was also linked to their thermal behavior based on a combination of lowest T_g, T_m, T_{cc}, and enthalpy of fusion (ΔH_f) values compared to other samples.

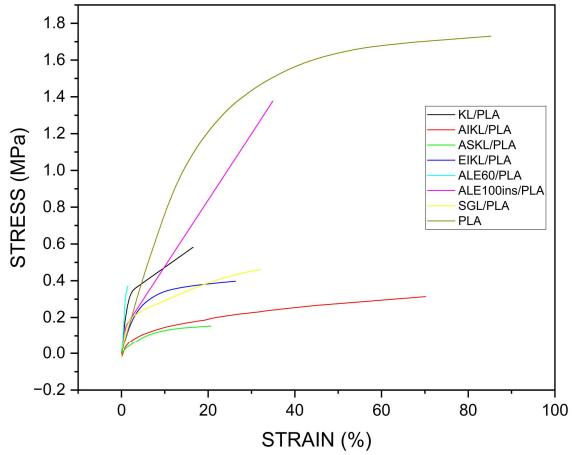


Figure 8. Figure of comparison of stress/strain curves of all samples tested (including the PLA control).

Young's modulus showed a strong positive correlation with the S/G ratio ($r = 0.74$) and T_{cc} ($r = 0.65$) and a negative correlation with T_m ($r = -0.64$). Alcell lignins were characterized by the highest Young's modulus and lowest elongation at break values, with ALE60/PLA, which had the highest Young's modulus of all samples and the lowest elongation at break, exhibiting almost entirely brittle behavior, with no apparent plastic behavior before the breakpoint (Table 3). This may be explained by the high S/G ratios found in hardwood lignin (Table 1), which gives it a more linear structure, making it more rigid than the softwood and herbaceous lignin, characterized by a more branched structure [38]. In contrast, KL/PLA showed both a low Young's modulus and low elongation at break (Table 3). The brittleness and rigidity of samples, which contain high-S/G ratio lignin, stem from the presence of fewer molecular chain entanglements, while fiber mats containing low-S/G lignin are characterized by a higher degree of branching, leading to an increase in chain entanglement, simultaneously improving mat flexibility.

In comparison, fractionated KL samples had the lowest Young's modulus values, but a high elongation at break (Table 3). This shows that using KL fractions resulted in fiber mats that are a lot more ductile and stretch more before breaking, despite a drop in mechanical strength.

It is important to note the moderate variance in fiber mat thickness across the samples resulting from the use of a stationary electrospinning setup. However, no correlations between the variance in thickness and mechanical properties were found ($r = -0.23$, -0.15, and -0.37 for the relationship between thickness and tensile strength; Young's modulus; and elongation at break, respectively).

In general, mechanical properties of switchgrass-derived CELF lignin were the most optimal for applications where good strength, flexibility, and dimensional stability is required, due to an excellent tensile strength, a low modulus, and a mid-to-high elongation at break. Similar properties were also observed in softwood-derived KL samples, while the use of hardwood-derived Alcell lignin resulted in drastically different mechanical properties, forming stiff fiber mats with little elongation.

3.5. Contact Angle

Neat PLA and lignin are both hydrophobic, and in nearly every case, adding lignin to PLA increased the hydrophobicity of fiber mats (Table 3; Figure 9). Most notably, the samples containing ALE60 and the neat KL and SGL exhibited the strongest hydrophobic performance, approaching superhydrophobicity (≥150°) (Figure 9). The soluble and insoluble fractions of various lignin sources using different solvents did not appear to have a consistent trend of increasing hydrophobicity—for example, AIKL did not increase contact angle significantly, while ASKL did by ~15°, and conversely, ESKL did not significantly increase contact angle while EIKL did, also by ~15° (Table 3; Figure 9). This might be due to the difference in the hydrogen bonding capacity of both solvents (δ_H = 19.4 for ethanol and δ_H = 7.0 for acetone), connecting ethanol's higher hydrogen bonding capacity with the more hydrophilic behavior of ESKL [28]. Additionally, acetone-insoluble Kraft lignin was found to be more hydrophilic than the soluble fraction (Table 3), most likely due to a comparatively higher relative total hydroxyl group content [26].

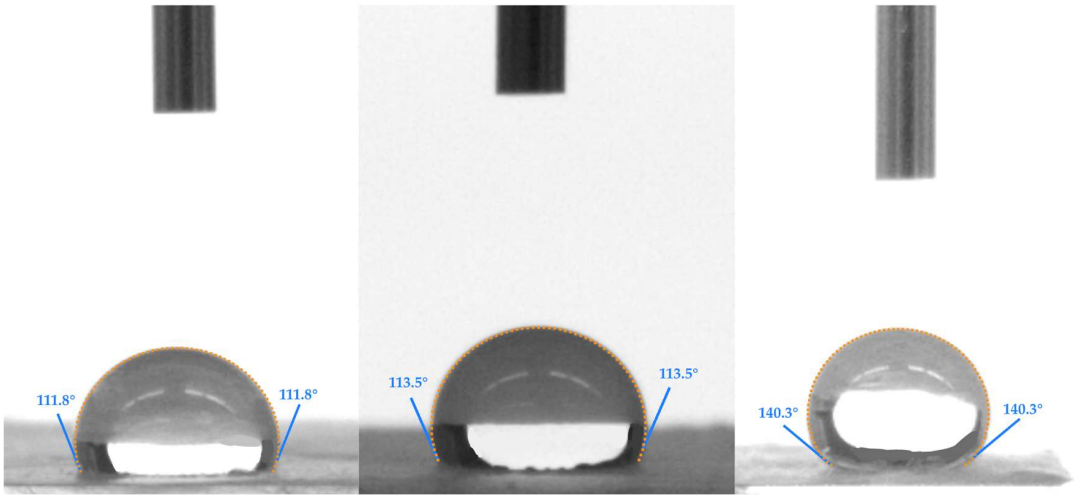


Figure 9. From left to right, sample water contact angle measurements of ESKL/PLA, neat PLA, and ALE60/PLA.

While the Alcell lignin-containing samples did not show any clear patterns, ALE60/PLA and ALE100ins/PLA had the highest contact angle measurements across all samples. Overall, the hydrophobic performance of samples with the highest contact angle measurements (KL/PLA, ASKL/PLA, EIKL/PLA, ALE60/PLA, ALE100ins/PLA, and SGL/PLA) seems to correlate with their thermal properties, particularly with the higher T_g values (r = 0.45), and exhibits a moderate inverse correlation with the relative total hydroxyl group content (r = −0.43). Finally, it is expected that the surface roughness and rigidity of the produced fiber mats also had a significant impact on the hydrophobicity of the samples, driven by strong correlation with their Young's modulus (r = 0.79).

The use of neat KL and SGL is the most efficient way to increase hydrophobic performance of a blend in fibers, eliminating the additional fractionation step. However, there is

a strong indication of increased hydrophobic performance originating from the samples containing hardwood Alcell lignin, and hence, further research with regard to solvent type and concentration during fractionation is necessary to optimize these parameters for fiber applications.

3.6. Antioxidant Properties

While studies show that antioxidant properties in lignin depend on its plant source and extraction method, the differences stemming from the different pretreatments were found to play the major role in determining lignin material's antioxidant capacity [62].

The presence of phenolic OH groups in lignin, which act as stabilizers in oxygen-induced reactions, was shown to be responsible for its antioxidant properties [63–65]. There are four types of phenolic OH groups with different reactivities found in different lignin structural units: syringyl, noncondensed and condensed guaiacyl, and *p*-hydroxyphenyl [66]. Hence, the biomass origin of lignin will dictate phenolic OH content based on its composition, and the lignin extraction method can further alter it.

All lignin samples showed immediate initial antioxidant activity within 5 min after the addition of 60 M DPPH solution in MeOH (Table 3). Pure DPPH-MeOH solution was used as a negative control and ascorbic acid as a positive control. Samples that contained KL or its fractions showed the highest antioxidant activity, which is in alignment with the findings that Kraft lignin tends to possess the highest number of phenolic hydroxyl groups. More specifically, AIKL/PLA and ASKL/PLA had the highest initial activity, with the color of the sample after initiation of the assay being close to the color of the ascorbic acid sample (Figure 10). Interestingly, some studies show that ASKL contains more phenolic OH groups than AIKL, which clearly relates to the higher antioxidant activity for ASKL/PLA between the two samples [26]. The relative magnitude of the FTIR peak at 1265 cm^{-1} (representing the C-O stretching of the G ring) correlates with these results, with highest values recorded for KL and its fractions, followed by SGL, and ending with lowest values for Alcell lignin samples. Additionally, relative S/G ratios of all samples showed a strong negative correlation coefficient (−0.84) with antioxidant activity, showing an inverse relationship between the two, further reinforcing the importance of G unit presence in the structure for excellent antioxidant performance. The exceptional antioxidant activity of KL and KL fraction samples is most likely due to the condensation reactions of lignin structure during Kraft pulping, yielding hard-to-decompose C-C bonds and new phenolic compounds [38], further underlining the impact of the extraction method on the chemical structure of lignin.

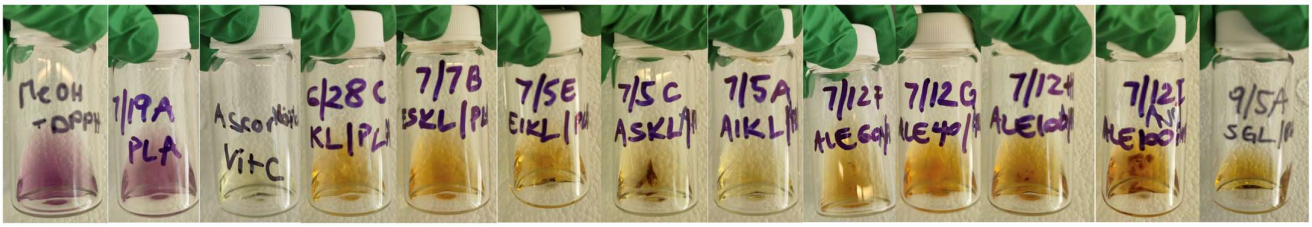


Figure 10. Different lignin/PLA nanofibers, neat PLA nanofibers, and ascorbic acid as positive control,5 min after the addition of 60 µM DPPH solution to MeOH, and DPPH/MeOH solution as negative control.

4. Conclusions

This study successfully demonstrated electrospinning of flexible lignin/PLA micro- and nanofiber mats, incorporating lignins of different origins, isolation methods, and post-

processing, and compared the structural, thermal, mechanical, and functional differences between these samples. The key findings are summarized as follows:

(1) Lignin addition to PLA in biocomposite fiber mats resulted in increased electrical conductivity and fiber diameter, reduced tensile strength, elongation at break, and thermal transition temperature, as well as increased hydrophobicity, with the latter showing a correlation with the T_g.
(2) Thermal properties of lignin/PLA samples were influenced by the hydroxyl content in lignin and inversely related to its degree of crosslinking. However, thermal values showed minimal variance across samples after lignin addition.
(3) Mechanical properties greatly varied by lignin type.
(4) While antioxidant activity was strong in all samples, it was highest in KL and its fractions due to the highly alkaline conditions in Kraft pulping, which correlated with phenolic OH content and, inversely, with the S/G ratio.
(5) KL/PLA and its fractions, EIKL/PLA and ASKL/PLA, exhibited high hydrophobicity, while KL/PLA and EIKL/PLA also showed high tensile strength; ASKL/PLA was characterized by a small fiber diameter, and the ESKL/PLA suspension had the highest electrical conductivity.
(6) SGL/PLA showed a small fiber diameter, as well as the highest tensile strength, coupled with a moderate modulus and elongation.
(7) Alcell/PLA samples showed the largest fiber diameters, with ALE60/PLA exhibiting the lowest elongation at break and the highest Young's modulus, as well as the highest hydrophobicity, followed closely by ALE100ins/PLA, which also had the lowest conductivity in the suspension of all samples.

This study showed that fractionation of lignin is not necessary for the purpose of achieving fiber spinnability, as was the case with the KL/PLA and SGL/PLA samples. Flexible low-cost nanofiber mats with good functional properties can be, therefore, obtained through a relatively fast, simple process without the use of heat. For example, SGL/PLA fiber mats can be used in cost-efficient air filtration applications, where ductility and a small fiber diameter are of essence. Alcell lignins/PLA fibers would be suitable for water filtration and packaging systems where barrier properties, rigidity, and dimensional stability are important. KL/PLA systems could be applied in biomedical products, such as in drug delivery wound dressings, as well as in cosmetic care, such as in therapeutic face sheet masks, where antioxidant benefits and ductility are valued.

However, fractionation of lignin can help tailor functional properties of such nanofiber mats for specific end use. For example, insoluble Alcell lignin/PLA fibers can be applied in battery separator membranes and supercapacitors where thermal stability, hydrophobicity, and electrical insulation are necessary. Fibers containing soluble fractions of KL, on the other hand, could be utilized in biosensors or other e-textile systems, in which electrical conductivity is required.

While these findings present many opportunities, further research is needed to scale lignin valorization effectively. First and foremost, the standardization of lignin as a feedstock is essential to ensure consistent quality and performance. In particular, the production of lignin/PLA biocomposite fibers requires a robust multivariate analysis that considers lignin isolation methods, biomass origins, and fraction, along with their corresponding physical and chemical properties. In terms of fiber formation, the use of non-stationary electrospinning setups could offer improved control over fiber mat uniformity and thickness. To address challenges in mechanical performance, modification of lignin/PLA blends or post-treatments—such as crosslinking—should be explored to enhance mechanical properties. Additionally, developing fiber systems that incorporate custom lignin blends tailored for multifunctional performance may unlock new levels of optimization. These

approaches would support efficient lignin utilization and enable property-driven synthesis for advanced applications.

Supplementary Materials: The following supporting information can be downloaded at: https://www.mdpi.com/article/10.3390/fib13090129/s1, Figure S1: Histogram of fiber diameter distributions for all lignin/PLA samples and neat PLA sample.

Author Contributions: Conceptualization, M.W.F. and D.B.S.; methodology, M.W.F. and D.B.S.; software, D.B.S. and E.L.F.; validation, M.W.F. and D.B.S.; formal analysis, D.B.S. and E.L.F.; investigation, M.W.F.,D.B.S. and E.L.F.; resources and data curation, M.W.F. and D.B.S.; writing—original draft preparation, D.B.S. and E.L.F.; writing—review and editing, M.W.F. and D.B.S.; visualization, D.B.S. and E.L.F.; supervision, M.W.F.; project administration, M.W.F.; funding acquisition, M.W.F. All authors have read and agreed to the published version of the manuscript.

Funding: This research received no external funding.

Data Availability Statement: The original contributions presented in this study are included in the article. Further inquiries can be directed at the corresponding authors.

Acknowledgments: This work made use of the Cornell Center for Materials Research Facilities. The authors are grateful to Chang Geun Yoo, Jiae Ryu, and Nara Han at SUNY College of Environmental Science and Forestry for supporting Alcell lignin processing and to Stephen Chmely and James Akor Godwin (Pennsylvania State University) for providing a sample of CELF switchgrass lignin for this study. This project was funded by the College of Human Ecology, Cornell University.

Conflicts of Interest: The authors declare no conflicts of interest.

Abbreviations

The following abbreviations are used in this manuscript:

CELF	Co-solvent Enhanced Lignocellulosic Fractionation
AIKL	Acetone-Fractionated Insoluble Kraft Lignin
ALE40	Alcell (40%) Ethanol-Soluble Lignin
ALE60	Alcell (60%) Ethanol-Soluble Lignin
ALE100	Alcell (100%) Ethanol-Soluble Lignin
ALE100Ins	Alcell (100%) Ethanol-Insoluble Lignin
ASKL	Acetone-Fractionated Soluble Kraft Lignin
DCM	Dichloromethane
DMA	Dynamic Mechanical Analysis
DMF	N,N-dimethyl formamide
DPPH	2,2-Diphenyl-1-picrylhydrazyl
DSC	Differential Scanning Calorimetry
EIKL	Ethanol-Fractionated Insoluble Kraft Lignin
ESKL	Ethanol-Fractionated Soluble Kraft Lignin
EtOH	Ethanol
FTIR	Fourier Transform Infrared Spectroscopy
G UNIT	Guaiacyl
H UNIT	p-hydroxyphenyl
PLA	polylactic acid
SGL	switchgrass lignin
S UNIT	syringyl

References

1. Sharma, S.; Sharma, A.; Mulla, S.I.; Pant, D.; Sharma, T.; Kumar, A. Lignin as Potent Industrial Biopolymer: An Introduction. In *Lignin: Biosynthesis and Transformation for Industrial Applications*; Springer: Cham, Switzerland, 2020; pp. 1–15. [CrossRef]
2. Ayyachamy, M.; Cliffe, F.E.; Coyne, J.M.; Collier, J.; Tuohy, M.G. Lignin: Untapped biopolymers in biomass conversion technologies. *Biomass Convers. Biorefinery* **2013**, *3*, 255–269. [CrossRef]

3. Sameni, J.; Krigstin, S.; Sain, M. Solubility of Lignin and Acetylated Lignin in Organic Solvents. *Bioresources* **2017**, *12*, 1548–1565. [CrossRef]
4. Wang, S.; Bai, J.; Innocent, M.T.; Wang, Q.; Xiang, H.; Tang, J.; Zhu, M. Lignin-based carbon fibers: Formation, modification and potential applications. *Green Energy Environ.* **2022**, *7*, 578–605. [CrossRef]
5. Choi, J.-H.; Cho, S.-M.; Kim, J.-C.; Park, S.-W.; Cho, Y.-M.; Koo, B.; Kwak, H.W.; Choi, I.-G. Thermal Properties of Ethanol Organosolv Lignin Depending on Its Structure. *ACS Omega* **2021**, *6*, 1534–1546. [CrossRef]
6. Meng, X.; Bhagia, S.; Wang, Y.; Zhou, Y.; Pu, Y.; Dunlap, J.R.; Shuai, L.; Ragauskas, A.J.; Yoo, C.G. Effects of the advanced organosolv pretreatment strategies on structural properties of woody biomass. *Ind. Crop. Prod.* **2020**, *146*, 112144. [CrossRef]
7. Wang, Y.-Y.; Sengupta, P.; Scheidemantle, B.; Pu, Y.; Wyman, C.E.; Cai, C.M.; Ragauskas, A.J. Effects of CELF Pretreatment Severity on Lignin Structure and the Lignin-Based Polyurethane Properties. *Front. Energy Res.* **2020**, *8*, 149. [CrossRef]
8. Yong, K.J.; Wu, T.Y. Recent advances in the application of alcohols in extracting lignin with preserved β-O-4 content from lignocellulosic biomass. *Bioresour. Technol.* **2023**, *384*, 129238. [CrossRef]
9. Gosselink, R.; Abächerli, A.; Semke, H.; Malherbe, R.; Käuper, P.; Nadif, A.; van Dam, J. Analytical protocols for characterisation of sulphur-free lignin. *Ind. Crop. Prod.* **2004**, *19*, 271–281. [CrossRef]
10. Abdelaziz, O.Y.; Hulteberg, C.P. Physicochemical Characterisation of Technical Lignins for Their Potential Valorisation. *Waste Biomass Valorization* **2017**, *8*, 859–869. [CrossRef]
11. Mariana, M.; Alfatah, T.; Abdul Khalil, H.P.S.; Yahya, E.B.; Olaiya, N.; Nuryawan, A.; Mistar, E.; Abdullah, C.; Abdulmadjid, S.; Ismail, H. A current advancement on the role of lignin as sustainable reinforcement material in biopolymeric blends. *J. Mater. Res. Technol.* **2021**, *15*, 2287–2316. [CrossRef]
12. Yoo, C.G.; Ragauskas, A.J. Opportunities and Challenges of Lignin Utilization. In *Lignin Utilization Strategies: From Processing to Applications*; American Chemical Society: Washington, DC, USA, 2021; pp. 1–12. [CrossRef]
13. Dallmeyer, I.; Ko, F.; Kadla, J.F. Correlation of Elongational Fluid Properties to Fiber Diameter in Electrospinning of Softwood Kraft Lignin Solutions. *Ind. Eng. Chem. Res.* **2014**, *53*, 2697–2705. [CrossRef]
14. Xue, J.; Wu, T.; Dai, Y.; Xia, Y. Electrospinning and electrospun nanofibers: Methods, materials, and applications. *Chem. Rev.* **2019**, *119*, 5298–5415. [CrossRef] [PubMed]
15. Dallmeyer, I.; Ko, F.; Kadla, J.F. Electrospinning of Technical Lignins for the Production of Fibrous Networks. *J. Wood Chem. Technol.* **2010**, *30*, 315–329. [CrossRef]
16. Attia, A.A.M.; Abas, K.M.; Nada, A.A.A.; Shouman, M.A.H.; Šišková, A.O.; Mosnáček, J. Fabrication, Modification, and Characterization of Lignin-Based Electrospun Fibers Derived from Distinctive Biomass Sources. *Polymers* **2021**, *13*, 2277. [CrossRef] [PubMed]
17. Poursorkhabi, V.; Mohanty, A.K.; Misra, M. Electrospinning of aqueous lignin/poly(ethylene oxide) complexes. *J. Appl. Polym. Sci.* **2015**, *132*, 41260. [CrossRef]
18. Cintra, I.L.R.; Rezende, M.C.; Guerrini, L.M.; Nahra, L.R.; Lucas, R.R.; Montagna, L.S.; Botelho, E.C. Electrospinning of PAN/lignin blends aiming the production of carbon nanofibers. *MRS Commun.* **2023**, *14*, 82–89. [CrossRef]
19. Gordobil, O.; Egüés, I.; Llano-Ponte, R.; Labidi, J. Physicochemical properties of PLA lignin blends. *Polym. Degrad. Stab.* **2014**, *108*, 330–338. [CrossRef]
20. Casasola, R.; Thomas, N.L.; Trybala, A.; Georgiadou, S. Electrospun poly lactic acid (PLA) fibres: Effect of different solvent systems on fibre morphology and diameter. *Polymer* **2014**, *55*, 4728–4737. [CrossRef]
21. Liang, R.; Yang, X.; Yew, P.Y.M.; Sugiarto, S.; Zhu, Q.; Zhao, J.; Loh, X.J.; Zheng, L.; Kai, D. PLA-lignin nanofibers as antioxidant biomaterials for cartilage regeneration and osteoarthritis treatment. *J. Nanobiotechnol.* **2022**, *20*, 327. [CrossRef]
22. Kim, D.; Bahi, A.; Liu, L.-Y.; Bement, T.; Rogak, S.; Renneckar, S.; Ko, F.; Mehrkhodavandi, P. Poly(Lactide)-Modified Lignin Nanofibers: Investigating the Role of Polymer Tacticity on Fiber Properties and Filtration Efficiency. *ACS Sustain. Chem. Eng.* **2022**, *10*, 2772–2783. [CrossRef]
23. Mushtaq, M.; Ahad, S.A.; Beaucamp, A.; Kumar, A.; Leite, M.M.; Hanrahan, J.P.; McGrath, J.; Singh, S.; Morris, M.A.; Geaney, H.; et al. Understanding the Importance of the Lignin–Biopolymer Ratio in Optimizing the Performance of Sustainable Biomass-Derived Electrospun Carbon Fiber Anodes in Sodium-Ion Batteries. *ACS Appl. Energy Mater.* **2025**, *8*, 8963–8972. [CrossRef]
24. Culebras, M.; Geaney, H.; Beaucamp, A.; Upadhyaya, P.; Dalton, E.; Ryan, K.M.; Collins, M.N. Bio-derived Carbon Nanofibres from Lignin as High-Performance Li-Ion Anode Materials. *ChemSusChem* **2019**, *12*, 4516–4521. [CrossRef]
25. Li, Q.; Hu, C.; Li, M.; Truong, P.; Li, J.; Lin, H.-S.; Naik, M.T.; Xiang, S.; Jackson, B.E.; Kuo, W.; et al. Enhancing the multi-functional properties of renewable lignin carbon fibers via defining the structure–property relationship using different biomass feedstocks. *Green Chem.* **2021**, *23*, 3725–3739. [CrossRef]
26. Karaaslan, M.A.; Cho, M.J.; Liu, L.Y.; Wang, H.; Renneckar, S. Refining the Properties of Softwood Kraft Lignin with Acetone: Effect of Solvent Fractionation on the Thermomechanical Behavior of Electrospun Fibers. *ACS Sustain. Chem. Eng.* **2021**, *9*, 458–470. [CrossRef]

27. Wetcha, P.; Aussawasathien, D.; Srithongkam, S.; Sowasod, N.; Naewkanya, P.; Tanthapanichakoon, W. Development for preparation of nanofibers using polylactic acid and biomass lignin via electrospinning process. *AIP Conf. Proc.* **2022**, *2440*, 030011. [CrossRef]
28. Ponnuchamy, V.; Gordobil, O.; Diaz, R.H.; Sandak, A.; Sandak, J. Fractionation of lignin using organic solvents: A combined experimental and theoretical study. *Int. J. Biol. Macromol.* **2021**, *168*, 792–805. [CrossRef] [PubMed]
29. Boeriu, C.G.; Bravo, D.; Gosselink, R.J.A.; van Dam, J.E.G. Characterisation of structure-dependent functional properties of lignin with infrared spectroscopy. *Ind. Crop. Prod.* **2004**, *20*, 205–218. [CrossRef]
30. del Río, J.C.; Gutiérrez, A.; Rodríguez, I.M.; Ibarra, D.; Martínez, Á.T. Composition of non-woody plant lignins and cinnamic acids by Py-GC/MS, Py/TMAH and FT-IR. *J. Anal. Appl. Pyrolysis* **2007**, *79*, 39–46. [CrossRef]
31. Sammons, R.J.; Harper, D.P.; Labbé, N.; Bozell, J.J.; Elder, T.; Rials, T.G. Characterization of Organosolv Lignins using Thermal and FT-IR Spectroscopic Analysis. *Bioresources* **2013**, *8*, 2752–2767. [CrossRef]
32. Popescu, C.-M.; Vasile, C.; Popescu, M.-C.; Singurel, G.; Popa, V.I.; Munteanu, B.S. Analytical methods for lignin characterization. II. Spectroscopic studies. *Cellul. Chem. Technol.* **2006**, *40*, 597–621.
33. Liu, R.; Dai, L.; Xu, C.; Wang, K.; Zheng, C.; Si, C. Lignin-Based Micro- and Nanomaterials and their Composites in Biomedical Applications. *ChemSusChem* **2020**, *13*, 4266–4283. [CrossRef] [PubMed]
34. Wang, Y.; Zhang, Y.; Cui, Q.; Feng, Y.; Xuan, J. Composition of Lignocellulose Hydrolysate in Different Biorefinery Strategies: Nutrients and Inhibitors. *Molecules* **2024**, *29*, 2275. [CrossRef] [PubMed]
35. Gandolfi, S.; Ottolina, G.; Riva, S.; Fantoni, G.P.; Patel, I. Complete Chemical Analysis of Carmagnola Hemp Hurds and Structural Features of Its Components. *Bioresources* **2013**, *8*, 2641–2656. [CrossRef]
36. de Souza Júnior, J.R.; Araujo, J.R.; Simão, R.A.; Archanjo, B.S. Cross-linked lignin coatings produced by uvlight and sf6 plasma treatments. In *Ciência e Engenharia de Materiais: Conceitos, Fundamentos e Aplicação*; Editora Científica Digital: Guarujá, Brazil, 2021; pp. 176–193. [CrossRef]
37. El Mansouri, N.-E.; Salvadó, J. Analytical methods for determining functional groups in various technical lignins. *Ind. Crop. Prod.* **2007**, *26*, 116–124. [CrossRef]
38. Jardim, J.M.; Hart, P.W.; Lucia, L.; Jameel, H. Insights into the Potential of Hardwood Kraft Lignin to Be a Green Platform Material for Emergence of the Biorefinery. *Polymers* **2020**, *12*, 1795. [CrossRef]
39. Kubo, S.; Kadla, J.F. Hydrogen Bonding in Lignin: A Fourier Transform Infrared Model Compound Study. *Biomacromolecules* **2005**, *6*, 2815–2821. [CrossRef]
40. Fiţigău, I.F.; Peter, F.; Boeriu, C.G. Structural Analysis of Lignins from Different Sources. *J. Mater. Metall. Eng.* **2013**, *4*, 167–172.
41. Mishra, P.K.; Ekielski, A. The Self-Assembly of Lignin and Its Application in Nanoparticle Synthesis: A Short Review. *Nanomaterials* **2019**, *9*, 243. [CrossRef]
42. Mann, D.G.J.; Labbé, N.; Sykes, R.W.; Gracom, K.; Kline, L.; Swamidoss, I.M.; Burris, J.N.; Davis, M.; Stewart, C.N. Rapid Assessment of Lignin Content and Structure in Switchgrass (*Panicum virgatum* L.) Grown Under Different Environmental Conditions. *Bioenergy Res.* **2009**, *2*, 246–256. [CrossRef]
43. Liu, Y.; Carriero, S.; Pye, K.; Argyropoulos, D.S. A Comparison of the Structural Changes Occurring in Lignin during Alcell and Kraft Pulping of Hardwoods and Softwoods. In *Lignin: Historical, Biological, and Materials Perspectives*; ACS Publications: Washington, DC, USA, 1999; pp. 447–464. [CrossRef]
44. Hosseinaei, O.; Harper, D.; Bozell, J.; Rials, T. Improving Processing and Performance of Pure Lignin Carbon Fibers through Hardwood and Herbaceous Lignin Blends. *Int. J. Mol. Sci.* **2017**, *18*, 1410. [CrossRef]
45. Tan, S.-H.; Inai, R.; Kotaki, M.; Ramakrishna, S. Systematic parameter study for ultra-fine fiber fabrication via electrospinning process. *Polymer* **2005**, *46*, 6128–6134. [CrossRef]
46. Attwenger, A. Value-Added Lignin Based Carbon Fiber from Organosolv Fractionation of Poplar and Switchgrass. Master's Thesis, University of Tennessee, Knoxville, TN, USA, 2014. Available online: https://trace.tennessee.edu/utk_gradthes/2768 (accessed on 24 March 2025).
47. Dastpak, A.; Louren, T.V.; Balakshin, M.; Hashmi, S.F.; Lundström, M.; Wilson, B.P. Solubility study of lignin in industrial organic solvents and investigation of electrochemical properties of spray-coated solutions. *Ind. Crop. Prod.* **2020**, *148*, 112310. [CrossRef]
48. Lora, J.H.; Glasser, W.G. Recent Industrial Applications of Lignin: A Sustainable Alternative to Nonrenewable Materials. *J. Polym. Environ.* **2002**, *10*, 39–48. [CrossRef]
49. Tanase-Opedal, M.; Ruwoldt, J. Organosolv Lignin as a Green Sizing Agent for Thermoformed Pulp Products. *ACS Omega* **2022**, *7*, 46583–46593. [CrossRef]
50. Kadla, J.F.; Kubo, S. Lignin-based polymer blends: Analysis of intermolecular interactions in lignin–synthetic polymer blends. *Compos. Part A Appl. Sci. Manuf.* **2004**, *35*, 395–400. [CrossRef]
51. Schlee, P.; Hosseinaei, O.; Keefe, C.A.O.; Mostazo-López, M.J.; Cazorla-Amorós, D.; Herou, S.; Tomani, P.; Grey, C.P.; Titirici, M.-M. Hardwood versus softwood Kraft lignin—Precursor-product relationships in the manufacture of porous carbon nanofibers for supercapacitors. *J. Mater. Chem. A Mater.* **2020**, *8*, 23543–23554. [CrossRef]

52. Vural, D.; Smith, J.C.; Petridis, L. Dynamics of the lignin glass transition. *Phys. Chem. Chem. Phys.* **2018**, *20*, 20504–20512. [CrossRef]
53. Sheridan, E.; Filonenko, S.; Volikov, A.; Sirviö, J.A.; Antonietti, M. A systematic study on the processes of lignin extraction and nanodispersion to control properties and functionality. *Green Chem.* **2024**, *26*, 2967–2984. [CrossRef]
54. Tanase-Opedal, M.; Espinosa, E.; Rodríguez, A.; Chinga-Carrasco, G. Lignin: A Biopolymer from Forestry Biomass for Biocomposites and 3D Printing. *Materials* **2019**, *12*, 3006. [CrossRef]
55. Kai, D.; Ren, W.; Tian, L.; Chee, P.L.; Liu, Y.; Ramakrishna, S.; Loh, X.J. Engineering Poly(lactide)-Lignin Nanofibers with Antioxidant Activity for Biomedical Application. *ACS Sustain. Chem. Eng.* **2016**, *4*, 5268–5276. [CrossRef]
56. Arasi, A.R.B.K.; Bengtsson, J.; Haque, M.; Theliander, H.; Enoksson, P.; Lundgren, P. Influence of Hardwood Lignin Blending on the Electrical and Mechanical Properties of Cellulose Based Carbon Fibers. *ACS Sustain. Chem. Eng.* **2024**, *12*, 11206–11217. [CrossRef] [PubMed]
57. El Mansouri, N.-E.; Yuan, Q.; Huang, F. Characterization of alkaline lignins for use in phenol-formaldehyde and epoxy resins. *Bioresources* **2011**, *6*, 2647–2662. [CrossRef]
58. Suota, M.J.; da Silva, T.A.; Zawadzki, S.F.; Sassaki, G.L.; Hansel, F.A.; Paleologou, M.; Ramos, L.P. Chemical and structural characterization of hardwood and softwood LignoForce^{TM} lignins. *Ind. Crop. Prod.* **2021**, *173*, 114138. [CrossRef]
59. Anwer, M.A.S.; Naguib, H.E.; Celzard, A.; Fierro, V. Comparison of the thermal, dynamic mechanical and morphological properties of PLA-Lignin & PLA-Tannin particulate green composites. *Compos. B Eng.* **2015**, *82*, 92–99. [CrossRef]
60. Guo, J.; Chen, X.; Wang, J.; He, Y.; Xie, H.; Zheng, Q. The influence of compatibility on the structure and properties of PLA/lignin biocomposites by chemical modification. *Polymers* **2020**, *12*, 56. [CrossRef]
61. Shi, K.; Liu, G.; Sun, H.; Weng, Y. Polylactic Acid/Lignin Composites: A Review. *Polymers* **2023**, *15*, 2807. [CrossRef]
62. Michelin, M.; Liebentritt, S.; Vicente, A.A.; Teixeira, J.A. Lignin from an integrated process consisting of liquid hot water and ethanol organosolv: Physicochemical and antioxidant properties. *Int. J. Biol. Macromol.* **2018**, *120*, 159–169. [CrossRef]
63. Eugenio, M.E.; Martín-Sampedro, R.; Santos, J.I.; Wicklein, B.; Ibarra, D. Chemical, Thermal and Antioxidant Properties of Lignins Solubilized during Soda/AQ Pulping of Orange and Olive Tree Pruning Residues. *Molecules* **2021**, *26*, 3819. [CrossRef]
64. Sadeghifar, H.; Argyropoulos, D.S. Correlations of the Antioxidant Properties of Softwood Kraft Lignin Fractions with the Thermal Stability of Its Blends with Polyethylene. *ACS Sustain. Chem. Eng.* **2015**, *3*, 349–356. [CrossRef]
65. Dong, X.; Dong, M.; Lu, Y.; Turley, A.; Jin, T.; Wu, C. Antimicrobial and antioxidant activities of lignin from residue of corn stover to ethanol production. *Ind. Crop. Prod.* **2011**, *34*, 1629–1634. [CrossRef]
66. Antonino, L.D.; Gouveia, J.R.; Júnior, R.R.D.S.; Garcia, G.E.S.; Gobbo, L.C.; Tavares, L.B.; dos Santos, D.J. Reactivity of aliphatic and phenolic hydroxyl groups in kraft lignin towards 4,4′ mdi. *Molecules* **2021**, *26*, 2131. [CrossRef]

Disclaimer/Publisher's Note: The statements, opinions and data contained in all publications are solely those of the individual author(s) and contributor(s) and not of MDPI and/or the editor(s). MDPI and/or the editor(s) disclaim responsibility for any injury to people or property resulting from any ideas, methods, instructions or products referred to in the content.